A study of ethanol conversion over zinc aluminate catalyst.

Gabriella Garbarino[1], Paola Riani[2], María Villa García[3], Elisabetta Finocchio[1], Vicente Sánchez Escribano[3] and Guido Busca[1*]

[1] Università degli Studi di Genova, Dipartimento di Ingegneria Civile, Chimica e Ambientale (DICCA), Laboratorio di chimica delle superfici e catalisi, P.le Kennedy, 1 16129 Genova, Italy

[2] Università degli Studi di Genova, Dipartimento di Chimica e Chimica Industriale (DCCI), Via Dodecaneso, 31 16146 Genova, Italy

[3] Departamento de Química Inorgánica, Universidad de Salamanca, Pl. de la Merced s/n, 37008 Salamanca, Spain.

Corresponding author

*phone +390103536024; fax +390103536028; e-mail: Guido.Busca@unige.it

Keywords: zinc aluminate, ethanol conversion, acetaldehyde, ethylene, diethylether, acido-basicity.

Abstract. The conversion of ethanol over a commercial $ZnAl_2O_4$ has been investigated. The catalyst has been fully characterized by XRD, IR, UV-Vis-NIR, ICP-OES, EDX-FE-SEM, BET and porosimetry. The catalyst is active in converting ethanol. At low conversion, diethyl ether is the main product while at higher conversions acetaldehyde is the main product (max yield ~ 50 %). Ethylene and ethylacetate are coproduced. Acetone and propylene become relevant products at complete conversion. The mechanism of formation of the products is discussed based on infrared surface chemical data, thermodynamic and kinetic data. Two independent catalytic sites exist, one for dehydration, the other for dehydrogenation, similar to those of Zinc oxide, giving rise to two parallel reaction sequencies. Criteria for developing selective catalysts towards dehydrogenation products are briefly discussed.

Introduction.

"Second generation bioethanol", i.e. ethanol produced by fermentation of lignocellulosics, could become a primary intermediate in the frame of a new industrial organic chemistry based on renewables [1,2]. Among the secondary intermediates potentially obtainable by converting (bio)ethanol, ethylene [3] and diethyl ether can be obtained by catalytic dehydration typically obtained over acidic catalysts [4], while acetaldehyde can be the primary product of ethanol dehydrogenation over metal catalysts (like Cu/ZnO [5]), bare ZnO being also reported to be active for such dehydrogenation [6,7]. Zn oxide-containing

catalysts have also been reported for the direct production of acetone [8] and ethylacetate [9], as well as butadiene [10] from ethanol. Early studies suggested catalysts based on ZnO-Al_2O_3 as highly efficient for butadiene synthesis from ethanol [11]. Coupling of acido-basic and de-hydrogenation properties are needed for catalyzing such complex reactions.

One of the best catalysts for ethanol dehydration is γ-Al_2O_3 [12,13], which allows yields of the order of 70-75 % in diethyl ether at ca 473 K and yield ~ 99 % in ethylene at temperatures in the range 573-623 K. Previous studies showed that the performances of alumina, although very good, are limited by the co-production of small amounts of higher hydrocarbons at high conversion, supposed to be due to the overconversion of ethylene [4,13,14,15]. A main point, additionally, is catalyst stability, due to the growth of carbonaceous materials that may progressively poison the catalyst [3], also reasonably due, at least in part, to acid-catalyzed overconversion of ethylene. Thus, doping or mixing of alumina with basic components could be beneficial. We did not find any dehydrogenation of ethanol on γ-Al_2O_3 in the absence of oxygen in the feed, in contrast to other authors which reported acetaldehyde formation [16,17], which could be associated to ethane formation by a hydrogen exchange process [17], and, maybe, also to the presence of impurities in the alumina catalyst [13,14,15].

On the other hand, according to the literature, alcohol dehydrogenation should be typically associated with catalyst basicity [18,19]. In fact, materials like basic zeolites [20] or calcined Mg-Al hydrotalcite [21] give rise to significant selectivities to acetaldehyde in the absence of oxygen, but only at low ethanol conversion. Industrial dehydrogenations of alcohols to carbonyl compounds are or have been performed also at the industrial level either over metal catalysts (mainly Cu-, Ag-based) or on transition metal oxides (such as zinc oxide), with high selectivity, but only at limited conversion with the recycling of unreacted ethanol [22,23]. Highly dispersed IB group metallic catalysts were shown to allow very high selectivity to acetaldehyde, but still at incomplete conversion [24,25].

To go deeper in the chemistry of ethanol on oxide surfaces, we investigated its conversion over stoichiometric zinc aluminate. Zinc aluminates, either stoichiometric or containing an excess of zinc, were characterized in earlier studies as basic materials [26,27]. In fact, ZnAl mixed oxides find practical application as catalysts for industrial processes, which have been classified as typically base-catalyzed. They are reported to act as the industrial catalysts of the Institut Français du Petrol (IFPEN) process for the biodiesel synthesis by transesterification of fats (Esterfip-H process [28,29]) as well as of polyethoxylation

processes producing non-ionic surfactants (Henckel, BASF [30,31]), and, as said, as promising systems for butadiene synthesis from ethanol [11]. Zinc aluminate has also been patented as an optimal catalyst for light olefins double bond position isomerization (Phillips [32]). $ZnAl_2O_4$ is also been reported to be an active photocatalyst [33] and a combustion catalyst [34]. Zinc aluminates are also supports or components of relevant industrial catalysts such as copper containing catalysts for methanol synthesis, low temperature water gas shift, hydrogen production through methanol steam reforming and, in particular, for dehydrogenations of alcohols [35].

In this paper we report both on the characterization of a commercial $ZnAl_2O_4$ spinel catalyst and on its behavior in the conversion of ethanol. Our interest on this material is on the structural similarity with defective spinel type aluminas, i.e. γ-Al_2O_3 and θ-Al_2O_3, as well as on the application of complex materials (such as Cu-Zn-Al systems) for ethanol conversion to useful products, in particular acetaldehyde.

Experimental

Materials

The catalyst used is a commercial Zinc aluminate (Puralox Zn44) manufactured by Sasol (44 wt% and 56 wt% of ZnO and alumina respectively with a surface area of 104 m^2/g). γ-Al_2O_3 (Puralox SBa200, 197 m^2/g)), θ-Al_2O_3 (Puralox SBa90, 90 m^2/g) and a home-made ZnO sample (31 m^2/g) were also used for comparison.

Material characterisation

XRD measure on the fresh catalyst was performed on a Siemens D-500 diffractometer (CuKα radiation, Ni filter; operated in the vertical mode at 40 kV and 30 mA) equipped with the Diffract AT V3 software package. The pattern was recorded over the 2θ angle ranging from 10° to 80° at a scan rate of 1.5 degree/min. XRD spectra on the spent catalyst was recorded on a Philips X'Pert MPD diffractometer with a Bragg-Brentano scattering geometry (Cu Kα). The diffraction pattern has been measured using a step of 0.02° and an acquisition time of 17 seconds.

BET surface area and porosity were measured using N_2 adsorption/desorption at 77 K determined volumetrically with a Micromeritics Gemini 2390a instrument. The sample has been previously outgassed at 383 K for 2 hours in N_2.

ICP-OES analysis was performed with a plasma emission spectrometer model Ultima II de Yobin Ivon. Samples for elemental analysis were obtained by treatment of 0.1 g of sample in HNO_3 + HCl + HF concentrated acid solution in a high pressure reactor.

DR-UVvisNIR spectra of both fresh and spent catalysts were collected with a JASCO V570 instrument equipped with an integrating sphere.

Qualitative and quantitative analyses were carried out by using a scanning electron microscope (SEM) Zeiss Evo 40 equipped with a Pentafet Link Energy Dispersive X-ray Spectroscopy (EDXS) system managed by the INCA Energy software (Oxford Instruments, Analytical Ltd., Bucks, U.K.). For qualitative and quantitative analyses, the samples were analyzed employing an acceleration voltage of 20 kV, using a Co standard for calibration in order to monitor beam current, gain and resolution of the spectrometer.

A Scanning Electron Microscope (SEM) Zeiss SUPRA 40 VP microscope, equipped with a field emission gun was used to investigate sample morphology. This instrument (FE-SEM) is equipped with a high sensitivity “InLens” secondary electron detector and with a EDX microanalysis OXFORD "INCA Energie 450x3". Sample powders were directly mounted on a high purity conductive double sided adhesive carbon tabs, or were suspended in ethanol under ultrasonic vibrations to decrease particle aggregation, then a drop of the resultant mixture was deposited on a copper tape and the dried sample was then imaged.

Pure powder pressed disks (20-30 mg) were activated in vacuum at 773 K in the IR cell (‘activated surface’) for one hour, then cooled down to liquid nitrogen temperature (77 K) and contacted with 10 torr of CO. The spectra of surface species were recorded in the presence CO and upon outgassing from 140 K up to room temperature (RT). Analogous pretreatment procedure has been followed for CO_2 adsorption test; in this case, the sample has been cooled down to room temperature and contacted with 35 Torr of spectroscopically pure CO_2 (from SIAD). The spectra of surface species were recorded in the presence of CO_2 gas at two different partial pressures, after outgassing at room temperature, and after outgassing up to 673 K.

IR spectra were recorded using Nicolet 380 FT-IR spectrometers. For skeletal studies, the samples were pressed into thin wafers with KBr and spectra were recorded in air. Spectra have been collected with 100 scans and a resolution of 2 cm^{-1}.

FT-IR studies of ethanol conversion were performed on compacted powder disks of 15-30 mg activated in vacuum at 773 K before adsorption experiments. Ethanol (several Torr)

was adsorbed at RT and spectra were recorded in the presence of the gas and at increasing temperature (473-773 K). In all cases, a Nexus ThermoNicolet instrument was used (OMNIC software, DTGS detector, 100 scans). All the spectra are reported in common scale.

Catalytic activity measures

Catalytic experiments were performed at atmospheric pressure in a tubular flow reactor (i.d. 7 mm) using different amounts of catalyst (0.25 - 1.25 g, 60-70 mesh sieved, thus achieving a ratio between the particle and internal reactor diameter near 25) and feeding ethanol (96% assay, from Sigma Aldrich) in nitrogen with a total flow rate of 80 cc/min. The carrier gas (nitrogen) was passed through a bubbler containing ethanol maintained at constant temperature (298 K) in order to obtain the desired partial pressures. The temperature in the experiment was varied stepwise from 423 K to 773 K.

Ethanol conversion is defined as usual:

$$X_{EtOH} = (n_{EtOH(in)} - n_{EtOH(out)})/n_{EtOH(in)}$$

while selectivity to product *i* is defined as follows:

$$S_i = n_i/(v_i(n_{EtOH(in)} - n_{EtOH(out)}))$$

where n_i is the moles number of compound *i*, and v_i is the ratio of stoichiometric reaction coefficients.

The contact time has been evaluated as the ratio of catalytic bed volume V (cm^3) on the effective flowrate Q (cm^3/s) at the working temperature, i.e. 623 K and 773 K.

Gas hourly space velocity has been calculated as the flow rate in STP (cm^3/h) divided by the catalytic bed volume (cm^3).

The outlet gases were analyzed by a gas chromatograph (GC) Agilent 4890 equipped with a Varian capillary column “Molsieve 5A/Porabond Q Tandem” and TCD and FID detectors in series. In order to identify the compounds of the outlet gases, a GC-MS Thermo Scientific with TG-SQC column (30 m x 0.25 mm x 0.25 μm) was used.

Results and discussion.

Bulk and morphological catalyst characterization.

In table 1 the results coming from manufacturer data and from EDX and ICP-OES analyses are reported. An excellent matching of analytic results with the producer's data have been found, corresponding with the typical composition of stoichiometric zinc aluminate, $ZnAl_2O_4$, confirmed as well by the Al/Zn atomic ratio that in all cases approaches 2. EDX data show the additional presence of some carbon (2.4% w/w) well distributed on the solid, likely due to carbonate species (see below).

FE-SEM micrographs (Figure S1) show that the catalyst particles have a blackberry-like morphology, with a primary particle size of the order of less than 20 nm, agglomerated in larger secondary particles. On the other hand, EDX/FE-SEM coupled analysis shows the presence of few small particles very rich in Zn, likely constituted by ZnO.

The measured BET surface area of the sample is 95 $m^2/g \pm 0.4$ m^2/g, value that roughly compares with the one given by the manufacturer (104 m^2/g). The nitrogen adsorption/desorption isotherm (Figure S2, left) correspond to the type IV of the IUPAC classification due to the presence of cylindrical pores with a width higher than 4 nm. The hysteresis loop is intermediate in between H1 and H2 [36], where pore structure is complex and in some way affected by network effects. A monomodal pore size distribution is observed (Figure S2, right) with a maximum frequencies of pore diameters between 4 and 9 nm, centered at 7 nm. The pore measured pore volume is 140 cm^3_{STP}/g corresponding to 0.217 cm^3/g when liquid nitrogen is considered.

XRD pattern of the fresh catalyst and of the exhaust catalyst, tested at 10000 h^{-1}, are reported in Figure S3. The fresh sample (in black) shows the typical feature of cubic $ZnAl_2O_4$ spinel (JCPDS No. 05–0669), as well as the spent one (grey difractogram). No other phases can be detected.

The skeletal IR spectrum (Figure S4, right) of the sample agrees well with that reported for the spinel $ZnAl_2O_4$ [37,38,39], with three IR active fundamentals found at 685, 553 and 492 cm^{-1}, the fourth IR active fundamental being expected near 225 cm^{-1}, i.e. out of the range of our measurement.

The DR-UV spectrum (Figure S4, left) shows a main maximum at 245 nm and a shoulder near 325 nm. The latter position (3.8 eV) well corresponds to the value reported in the literature for the direct VB $\rightarrow$ CB transition of bulk $ZnAl_2O_4$ particles [40] but is also in the region of the absorption of ZnO. On the other hand, the position of the main band (5.06 eV) corresponds closely to that reported by other authors for $ZnAl_2O_4$ nanoparticles [41]. In

fact, it is well known that the E_g values of nano-sized semiconductors increase with decreasing particle size. Thus, the main observed absorption in the UV spectrum is assigned to spinel nanoparticles, while the component at 325 nm is assigned to ZnO particles.

Surface catalyst characterization by IR spectroscopy.

The IR spectrum of the pure powder disk, after activation at 773K, is reported in Figure S5. The bands at 1465, 1420 cm^{-1} are due to residual carbonate species in a nearly trigonal form. The resistance of carbonate species to desorption is in line with the intrinsic significant basicity of $ZnAl_2O_4$ [26,27]. On the other hand, this datum indicates that, in practical conditions, these materials can work with a partially carbonated surface, i.e. with the strongest basic sites “poisoned” by carbonates and unavailable for the reaction. The presence of carbonates explains the detection of carbon homogeneously distributed on the sample, as evidenced by EDX analysis (see above).

In the region of the surface hydroxyl groups, a main IR band is observed at 3690 cm^{-1} that, in agreement with previous studies [27,42], can be assigned to Zn-OH groups. The features at higher frequencies, with a component near 3765 cm^{-1} are due to alumina-like hydroxyl groups [13,14,43,44].

The spectra of CO adsorbed at 140-273 K after previous outgassing activation at 773 K in the region 2040-2240 cm^{-1}, are presented in Figure 1. Two main bands at ca. 2173 and 2149 cm^{-1}, are observed after CO adsorption at 133 K. The lower frequency band disappears rapidly upon outgassing upon warming from 133 to 153 K. When this band is present, the spectrum of the surface OH groups is markedly modified, with the partial disappearance of the main band at 3690 cm^{-1}, and the appearance of a slightly broader component at 3615 cm^{-1}. Thus, the CO band at 2149 cm^{-1} can be confidently assigned to CO stretching of carbon monoxide H-bonded to the main surface hydroxyl groups of $ZnAl_2O_4$. The shift of the OH stretching band upon this interaction is relatively small ($\Delta\nu OH \sim 75$ cm^{-1}) indicating that the acidity of the main OH’s of $ZnAl_2O_4$ is weak. In particular, the shift is lower with respect to that found for the main OH stretching band of γ-Al_2O_3 ($\Delta\nu OH \sim 150$ cm^{-1}) indicating a lower protonic acidity of $ZnAl_2O_4$ than that found on γ-Al_2O_3 [43, 44]. The higher frequency band is actually formed by two components, one at 2173 cm^{-1} and the other at 2196 cm^{-1}: the former component, disappearing first by further outgassing upon warming, is not observed on aluminas [43,44], but its frequency is similar to that

observed at high coverages on ZnO [45]. It is assigned to CO interacting with Zn^{2+} ions. The second band is similar to the main one observed at high coverages on γ-Al_2O_3, but is not far from the position of surface carbonyls observed on ZnO at low coverages. A further small band is observed at 2240 cm^{-1} and it is due to CO interacting with highly exposed low coordination Al^{3+} cations, usually present in small amounts also on the γ-Al_2O_3 surfaces [43,44], where, however, significant absorption is usually found also in the region 2020-2000 cm^{-1}. These data indicate that several kinds of Lewis acid sites exist on the surface, both of the Al^{3+} type and of the Zn^{2+} type. However, it also indicates that a large part of strong Lewis sites present on the alumina surface are not observed on the $ZnAl_2O_4$ surface.

In Figure 2 the results arising from CO_2 adsorption experiment are summarized. When CO_2 is admitted in the IR cell several new bands appear at 2350 cm^{-1}, 1644 cm^{-1}, 1500 cm^{-1} and a split feature at 1237-1228 cm^{-1}. The band at 2350 cm^{-1} is due to CO_2 linearly adsorbed at the surface: it quickly disappears upon outgassing at 373 K. The bands at 1644, 1500, 1237 and 1228 cm^{-1} are assigned to monohydrogencarbonate species ($\nu_{as}COO^-$, $\nu_{sym}COO^-$, δOH modes). Similar bands were already reported after CO_2 adsorption on $ZnAl_2O_4$ [46], γ-Al_2O_3 and ZnO [47]. Conversely, the subtraction spectra show that OH's bands at 3760 cm^{-1}, 3735 cm^{-1} and 3692 cm^{-1} decrease markedly in intensity, likely due to the reaction of surface hydroxyl groups with CO_2. In parallel, a new sharp band at 3617 cm^{-1} appears due to νOH of monohydrogencarbonate species [47]. The formation of monohydrogencarbonate species in these conditions indicate that some basic / nucleophilic sites still exist on the surface, besides those involved in the formation of the residual carbonates that are not freed by outgassing at 773 K. The splitting of the δOH mode of monohydrogencarbonate species suggests that at least two types of monohydrogencarbonate species are present, likely one involving the OH's on Zn-OH sites and another involving Al-OH sites.

Catalytic activity in the flow reactor.

In Table 2 the data concerning the catalytic activity of the $ZnAl_2O_4$ catalyst in the conversion of ethanol at GHSV 10000 h^{-1} are reported and compared with that obtained at the same GHSV conditions over γ- and θ-Al_2O_3 and ZnO. Experiments have been realized using the same inlet feed composition but different GHSV (in the range 3514 h^{-1} - 20000 h^{-1}), and at different temperatures (423-773 K) in apparent steady state conditions. The data

obtained with different space velocities are compared in Fig. S6. At low temperature and conversion, independently from SV, two main products are observed: acetaldehyde and diethyl ether. By increasing the reaction temperature, diethyl ether selectivity decreases in all cases, while acetaldehyde selectivity increases first but decreases later, in particular at low GHSV. Ethylene and ethylacetate are also found: however, the former increases its selectivity with temperature at any SV, while the latter also has a maximum selectivity with increasing temperature. At high temperature, the catalyst gives rise to a number of other products such as propylene, acetone, CO_2, butanaldehyde, pentanone, several C4 hydrocarbons including small amounts of 1,3-butadiene, 1,4 pentadiene and benzene (reported as selectivity to other products, S Other).

In Figure 3 the effect of contact time τ on conversion and selectivities to the main products is reported at 623 K and 773 K. At 623 K as expected, the conversion of ethanol increases by increasing contact time. However, at 623 K, the selectivities to the five main products, diethyl ether, acetaldehyde, ethylene, ethylacetate and acetone, are rather independent from τ. Indeed, a slightly decreasing trend is found for diethyl ether selectivity, and this indicates a slightly decreasing diethyl ether to ethylene ratio with increasing conversion. At 773 K the conversion is very high or total for all tested τ. At this temperature acetaldehyde selectivity markedly drops progressively, at least in the range τ 0.05 ÷ 0.25 s, while also selectivities to ethylacetate and diethyl ether decrease. In contrast, selectivities to all other products increase, at least in the range τ 0.05 ÷ 0.25 s.

From the conversion data at low conversion, an evaluation of the apparent activation energies (E_{att}) was done. At higher space velocities, apparent E_{att} > 90 kJ/mol, showing that kinetic regime is prevalent. The measured E_{att} value, however, seems to decrease progressively by increasing contact time down to values E_{att} ~ 60 kJ/mol, still showing a chemical kinetic range. The moderate decrease of apparent E_{att} might be attributed either to an imperfect isothermal behaviour of the reactor, or to some influence of diffusional limitations.

A comparison can be made between the behavior of $ZnAl_2O_4$ with that of different aluminas, such as γ-Al_2O_3 and θ-Al_2O_3 , shown in Table 2, tested at GHSV 10000 h^{-1}. The surface area of the γ-Al_2O_3 sample is about 190 m^2/g, thus nearly the double than that of $ZnAl_2O_4$, while that of the θ-Al_2O_3 sample is near 90 m^2/g, i.e. a little lower than that of $ZnAl_2O_4$. It is evident that the catalytic activity of both Al_2O_3 samples is far higher than that

of $ZnAl_2O_4$, with significant conversion already at 473 K (producing diethyl ether only) and almost total conversion already at 573 K for γ-Al_2O_3 and at 623 K for θ-Al_2O_3, producing ethylene with very high selectivities. These data seem to indicate that the active sites for the production of diethyl ether are not only much more on aluminas than on zinc aluminate (higher activity at the same temperature), but also more active on aluminas than on zinc aluminate (activity at lower temperature). We also note that on aluminas ethylene becomes prevalent with respect to diethyl ether on alumina already at 573 K, while on $ZnAl_2O_4$ this only occurs at 773 K. On the other hand, the inversion diethyl ether versus ethylene selectivity occurs in all cases when ethanol conversion is higher than 80 %. This, together with the slight decrease of the diethyl ether to ethylene ratio by increasing τ found above, supports the previous statement that the ethanol dehydration reactions (balance between reactions (1) and (2), see below) are influenced strongly by ethanol conversion, i.e. by the availability of gas phase ethanol, as well as by the temperature. On the other hand, it is evident that, on $ZnAl_2O_4$, the dehydrogenation catalytic activity (absent on pure aluminas), strongly increasing with temperature, competes with the formation of ethylene at high temperature more than with the formation of diethyl ether at lower ones.

To complete the picture, the catalytic data obtained on $ZnAl_2O_4$ can also be compared with those obtained on ZnO. The data of our experiment performed at GHSV = 10000 h^{-1} on ZnO, also reported in table 2, are consistent with literature data [48]. In spite of the far lower surface area with respect to $ZnAl_2O_4$, ZnO is more active in converting ethanol than zinc aluminate. In particular, ZnO converts ethanol to acetaldehyde and its overcoversion products, acetone and CO_2, definitely more than $ZnAl_2O_4$, while it presents a similar activity than $ZnAl_2O_4$ in converting ethanol to diethyl ether at low temperature and to ethylene at high temperature.

Infrared study of the catalytic reaction.

The results of the experiment performed in the IR cell are reported in Figures 4 and 5. The gas phase spectra (Figure 4) show only ethanol (E) in the vapour phase up to 473 K, while small traces of acetaldehyde (A), ethylene (E=) and diethyl ether (D) appear simultaneously at 523 K. Comparison with a blank experiment confirm the catalytic effect of $ZnAl_2O_4$, because no reactivity is observed without it up to 573 K.

Ethanol is fully disappeared in the presence of the catalyst at 773 K, when acetone (Ac), propene (P), butene (B) are clearly observed together with acetaldehyde (A), ethylene

(E=), methane (M) and diethyl ether (D). The presence of ethylacetate cannot be excluded due to the superimposition of bands.

The spectra of the surface species on the catalyst during ethanol conversion are presented in Figure 5. The main bands at 1119 and 1072 cm^{-1} are attributed to the asymmetric and symmetric stretching modes of the C–C–O system of surface ethoxide species. The amount of undissociated adsorbed ethanol is very small, if at all. The band at 1167 cm^{-1} is essentially a CH_3 rocking mode also having a CO stretching character, while the maxima at 1450 cm^{-1} (δ_{as} CH_3) and 1390 cm^{-1} (δ_{sym} CH_3) are due to deformation modes of the CH_3 group to which the CH_2 scissoring mode is superimposed, due to the same ethoxy groups. The overall spectrum of ethoxy groups is similar to that observed on alumina [13]. A very weak broad band centered at 1297 cm^{-1}, due to the COH deformation mode of undissociated adsorbed ethanol, provides evidence of the presence of adsorbed undissociated species in very small amounts. By increasing the temperature, the spectrum is essentially unchanged up to 423 K. Two bands at 1575 and 1445 cm^{-1} appear very weak at 473 K and strong at 523 K, together with the doublet at 1346 and 1335 cm^{-1}. These bands are associated with acetate species. At 573 K the spectrum of acetate species shows most intense a band at 1620 cm^{-1}. It seems likely that two different acetate species form. At increasing temperatures (573-773 K), it seems evident that the surface alkoxide species progressively disappear from the surface while the bands of surface acetates are almost unchanged. In this temperature range, most products appear in the gas phase, suggesting that these products mainly involve ethoxide groups as surface intermediates.

Thermodynamic considerations

In Figure S7a, the theoretical conversion at equilibrium of the system ethanol / diethylether / water is reported, according to the following reactions

$$2\ CH_3CH_2OH \leftrightarrows (CH_3CH_2)_2O + H_2O \qquad (1)$$

$$CH_3CH_2OH \leftrightarrows H_2C{=}CH_2 + H_2O \qquad (2)$$

These calculations were done using the Redlich Kwong Soave equation of state and a Gibbs reactor, in the diluted conditions used in our experiments. Ethanol should be almost completely converted in the entire temperature range, with diethyl ether being the only C-product (together with water) at temperatures up to near 300 K, and ethylene the only C-product at temperatures above 480 K. In the intermediate temperature range, diethyl ether

and ethylene are coproduced. This shows that the dehydration reactions over $ZnAl_2O_4$ in our experimental conditions are kinetically hindered below 750 K, i.e. up when ethanol is still not completely converted and diethyl ether is still observed as a product.

In Figure S7b, the equilibrium of the dehydrogenation reaction of ethanol to acetaldehyde

$$CH_3CH_2OH \leftrightarrows H_3C\text{-}CHO + H_2 \qquad (3)$$

is considered, in our feed conditions. Conversion of ethanol should be already significant (> 75%) at 550 K, with nearly full yield of acetaldehyde above 700 K. Thus, also dehydrogenation is kinetically hindered in our conditions in the all space velocity range at least up to 700 K. By putting together the dehydration and dehydrogenation equilibria (Figure S7c), it becomes clear that dehydration products are far more favoured than dehydrogenation products in all the investigated temperature range. This shows that $ZnAl_2O_4$ catalyzes more efficiently the dehydrogenation reaction that the dehydration one, in contrast to Al_2O_3 samples that catalyze only the dehydration reactions, with no dehydrogenation activity.

In Figure S7d, the reaction producing acetone from acetaldehyde:

$$2\ CH_3CHO + H_2O \leftrightarrows CH_3COCH_3 + CO_2 + 2H_2 \quad (4)$$

has been also included in the equilibrium calculation, to account for the observed formation of acetone and CO_2. This reaction is definitely favored thermodynamically in our temperature range. It allows to decrease the equilibrium yield of acetaldehyde (as the reactant of this equilibrium) and ethylene (due to competition between parallel equilibria), with acetone becoming the most abundant carbon product together with ethylene. Interestingly at low temperature (T<580 K) the main expected product is ethylene followed by acetone, while at higher temperatures (T>580 K) a slight inversion in the corresponding yields is expected, being acetone main product with a maximum yield of 45% at equilibrium.

Characterization of the spent catalyst.

The UV-Vis spectra of the spent catalysts are compared in Figure 6 with those of the fresh catalyst. It is evident the growth of an absorption in the near UV and visible regions, likely associated to the deposition of carbonaceous materials. In agreement, the spent catalyst looks dark in color.

The FE-SEM-EDX data roughly indicate that the amount of carbon increases with time on stream from ~ 2.5 wt% on the fresh catalyst, to 8-40 wt% on the spent catalysts. On the other hand, C-rich particles are not evident in the FE-SEM images. Conversely, XRD analysis (Figure S3, grey pattern) does not show the presence of crystalline carbon species, indicating that carbon species would spread over the catalyst surface.

Discussion.

The characterization data discussed above confirm that the material under study is constituted essentially by a mixed oxide of Zn and Al, i.e. by the spinel $ZnAl_2O_4$. Very few ZnO-rich particles are also present according to EDX-FE-SEM analyses. The surface characterization also shows that the sample contains features typical of alumina, in particular Lewis acidic / low coordination Al^{3+} ions, and weakly nucleophilic sites forming monohydrogencarbonates upon CO_2 adsorption. Together, Zn^{2+} ions, weakly acidic Zn-OH groups and very basic sites are also present. IR data show that these carbonate species are strongly bonded, being not completely removed even by outgassing at 773 K. It seems consequently that at least a part of them remain on the surface during catalysis and poison the strongest basic sites which could not be available for the catalytic reaction. Thus, the surface shows indeed a pronounced character of a zinc oxide more that of a transitional alumina based material. This might be associated to the normal spinel character of $ZnAl_2O_4$, where Zn^{2+} occupies tetrahedral positions and Al^{3+} is essentially limited to octahedral positions. In fact, the presence of Al^{3+} in tetrahedral coordination makes transitional aluminas very acidic and very reactive materials.

The catalytic data reported here show that zinc aluminate nanopowder sample is active in converting ethanol, producing several products with moderate selectivities. Reactivity is significant above 500 K. At low conversion, the main products are diethyl ether and acetaldehyde, reasonably produced by reactions (1) and (3). This behavior is different from that of γ-Al_2O_3 and θ-Al_2O_3 where diethyl ether is the only product formed in the same conditions. In fact, the catalytic activity of aluminas, producing dehydration reactions to diethyl ether and ethylene, attributed to the surface Lewis acidity of these materials [43,44], is observed at definitely lower temperatures than on $ZnAl_2O_4$. Dehydrogenation activity of $ZnAl_2O_4$, not found on aluminas, is certainly associated to its nature of a Zn-containing mixed oxide. However, dehydrogenation activity of $ZnAl_2O_4$ is lower than that of ZnO, which also presents similar dehydration activities. The higher activity of ZnO in dehydrogenation to acetaldehyde and in its overconversion to acetone can be ascribed

possibly to the presence of Zn-O-Zn groups on ZnO, which do not exist in the spinel structure of $ZnAl_2O_4$. This activity might be associated to the ability of ZnO and of ZnO-containing materials to dissociatively adsorb hydrogen [49,50].

On the other hand, ZnO and $ZnAl_2O_4$ present also similar non-negligible catalytic activity in dehydrogenation, although well lower, as said, than that of aluminas. In fact, previous data showed that also materials characterized by significant basicity, like e.g. calcined hydrotalcite [21], produce significant yield in ethylene and diethylether together with acetaldehyde, upon ethanol conversion.

IR spectroscopy shows that ethanol essentially adsorbs in the form of ethoxy-groups on $ZnAl_2O_4$: it does not seem possible to distinguish different kinds of alkoxy groups. Ethoxy groups become active in the 500-600 K range producing, in parallel, diethyl ether and acetaldehyde. The formation of diethyl ether at low ethanol conversion is found on $ZnAl_2O_4$ and very likely involves the reaction of ethoxy groups with undissociatively adsorbed ethanol, as discussed elsewhere [51].

$$CH_3CH_2OH + M^{n+}\ {}^{=}O\ (surf) \leftrightarrows CH_3CH_2O^-\ M^{n+}\ {}^{-}OH\ (surf) \quad (5)$$

$$CH_3CH_2O^-\ M^{n+}\ {}^{-}OH\ (surf) + CH_3CH_2OH \leftrightarrows (CH_3CH_2)_2O + M^{n+}\ {}^{=}O\ (surf) + H_2O \quad (6)$$

As usual, the production of diethyl ether decreases with increasing temperature and contact time, while the one of ethylene starts to form with increasing selectivity. The main way to ethylene at high temperature is very likely associated to the monomolecular decomposition of ethoxide species on the same alumina-like sites.

$$CH_3CH_2O^-\ M^{n+}\ {}^{-}OH\ (surf) \leftrightarrows H_2C{=}CH_2 + M^{n+}\ {}^{=}O\ (surf) + H_2O \quad (7)$$

Both low coordination Zn^{2+} ions (coming from Zn^{2+} in un-complete tetrahedral coordination) and Al^{3+} ions (coming from Al^{3+} in un-complete octahedral coordination) can be responsible or such reactions, which occur at higher temperature than on alumina whose active sites are most likely Al^{3+} ions coming from Al^{3+} in un-complete tetrahedral coordination.

In contrast, the production of acetaldehyde occurs only around Zn^{2+} sites, taking into account the hydrogen adsorption ability of Zn^{2+} - O^{2-} couples. This would likely occurs too starting from ethanol adsorbed as ethoxy group on Zn^{2+} - O^{2-} ionic couples.

$$CH_3CH_2OH + Zn^{2+}\ {}^{=}O\ (surf) \leftrightarrows CH_3CH_2O^-\ Zn^{2+}\ {}^{-}OH\ (surf) \quad (8)$$

$CH_3CH_2O^-$ Zn^{2+} ^-OH (surf) ⇆ CH_3CHO + Zn^{2+} ^-H ^-OH (surf) ⇆ CH_3CHO + Zn^{2+} $^=O$ (surf) + H_2 (9)

The independence of the apparent reaction rate to acetaldehyde and to diethylether from contact time is in agreement with the existence of two different adsorption sites although producing similar surface intermediates.

Ethylacetate is also produced: it can reasonably be formed by the Tishchenko condensation of the same acetaldehyde

2 CH_3CHO ⇆ CH_3CO-O-CH_2CH_3 (10)

However, in this case the production of ethylacetate is expected to increase with contact time while that of acetaldehyde is expected to decrease with contact time. This is not found.

An alternative way to produce ethylacetate, suggested by IR spectroscopy results as well as by catalytic data, is the following:

CH_3CH_2OH + OH^-(surf) ⇆ $CH_3CO_2^-$ (surf) + 2 H_2 (11)

CH_3CH_2OH + $CH_3CO_2^-$ (surf) ⇆ $CH_3COOCH_2CH_3$ + OH^-(surf) (12)

Acetate species, well evident in IR spectra, clearly form already at 573 K on the surface but seem to be almost inactive in the IR experiments. It is possible that they react with ethanol in flow conditions (i.e. with a constant flow of unreacted ethanol) producing ethylacetate.

In contrast, the catalytic data suggest that acetone and propene are indeed produced from acetaldehyde, according to the behavior of the selectivities with respect to contact time. CO_2 is likely coproduced with these C3 molecules. Acetone is likely produced through aldol-like condensation of acetaldehyde followed by decarbonylation/dehydrogenation of acetaldol or decarboxylation/dehydrogenation of the corresponding hydroxy-acid. Propene could arise from crotonic condensation of acetaldehyde, followed by decarbonylation of crotonic aldehyde or decarboxylation of the corresponding acid.

Indeed, although this catalytic material shows significant activity and selectivity to acetaldehyde, with yield up to near 50 % at 773 K and SV 20000 h^{-1}, the selectivity to acetaldehyde is limited at low conversion by the formation of diethyl ether and at high conversion by the formation of a number of products such as ethylene, acetone,

ethylacetate and propene. On the other hand, in our conditions we did not obtain high selectivities to other useful products, such as e.g. butadiene, reported elsewhere to be a main product over a similar catalyst [11]. Thus, we can suppose that the combination of acid-base and dehydrogenating properties of this catalyst is not good enough to produce molecules expected to arise from complex step mechanisms, at least in the conditions used here.

From the data it appears that to produce ethanol dehydrogenation products, such as acetaldehyde and, may be other such as ethylacetate, it is necessary to really not have or kill the Lewis acid-based dehydration activity to diethyl ether and ethylene. In fact, ethanol dehydration reactions are much more favoured thermodynamically than dehydrogenation ones, and are easily catalyzed not only by strong Lewis acid centers, but possibly also by quite basic surfaces.

The analyses on the $ZnAl_2O_4$ spent catalysts show the growth, at least at the beginning of the reaction, of carbon species, detected by EDX, and of species absorbing in the visible range detected by UV-vis-NIR spectroscopy as well as by visual inspection. Interestingly, however, FE-SEM microscopy does not reveal the presence of C-rich particles. It is concluded that carbon rich molecular units, such as e.g. polyaromatic species, should form at the surface of the catalyst.

Conclusions.

The data reported here show that zinc aluminate spinel, at least without strong previous activation treatments, is an active catalyst for converting ethanol, but lacks of selectivity. In particular acetaldehyde yield up to near 50 % at 773 K and SV 20000 h^{-1} is obtained: however, selectivity to acetaldehyde is affected by diethyl ether production at low conversion, and by the formation of several products (i.e. ethylene, acetone, propene and others) at high conversion. Some carbon species form on the catalyst surface but they are homogeneously distributed on the surface without producing evident C-rich particles. On the other hand, no deactivation is observed at the one-day time on stream scale.

Kinetic data show that dehydration and dehydrogenation routes are parallel: dehydration to diethyl ether and ethylene occurs on Lewis acidic alumina-like sites while dehydrogenation to acetaldehyde occurs on Zn-oxide like sites. Acetaldehyde is apparently intermediate in

the production of acetone and propene, probably through previous aldol condensation, while ethylacetate is probably formed through surface acetate and undissociated ethanol.

Thermodynamic evaluations show that dehydration reactions are much more favored than dehydrogenation at T < 773 K, and that further conversion of acetaldehyde to acetone is strongly favoured in this range. Thus, to have very high yields to acetaldehyde it is necessary to kill the dehydration route and also the aldol condensation activity. This means that acido-basic activity of the catalyst should be minimal.

Acknowledgement

The authors would like to acknowledge Antonio Bacigalupo and Michele Pastorino for performing the catalytic tests during their Bachelor's thesis.

Table 1: elemental composition from manufacturer, EDX and ICP-OES analysis.

Data	Zn wt%	Al wt%	O wt%	C wt%	Al/Zn atomic ratio
Manufacturer	35.3 %	29.6 %	35.0%	n.a.	2.03
EDX	31.0%	25.0%	41.5%	2.5%	1.95
ICP-OES	34.74%	28.82%	n.a.	n.a.	2

Table 2. Ethanol conversion and selectivity (S) to C-containing products of ethanol at GHSV = 10000 h^{-1}.

Catalyst	Temperature (K)	Ethanol conversion (%)	$(C_2H_5)_2O$	C_2H_4	Other HC	CH_3CHO	CH_3COCH_3	CO_2	Other oxyg.
γ-Al_2O_3	423	0.2	100	-	-	-	-	-	-
	473	20.8	99.1	0.9	-	-	-	-	-
	523	78.6	79.7	20.2	0.1	-	-	-	-
	573	97.7	0.3	99.7	0	-	-	-	-
	623	99.7	0	100	0	-	-	-	-
	673	99.9	0	99.8	0.1	-	-	-	-
	723	100	0.1	98.9	0.8	-	-	-	-
θ-Al_2O_3	423	0	-	-	-	-	-	-	-
	473	5.3	100	0	0	-	-	-	-
	523	66.6	93.2	6.8	0	-	-	-	-
	573	85.6	67.7	32	0	-	-	-	-
	623	100	0	99.4	0.6	-	-	-	-
	673	100	0	99.6	0.4	-	-	-	-
	723	100	0	98.8	1.2	-	-	-	-
$ZnAl_2O_4$	473	0	-	-	-	-	-	-	-
	523	0.6	73.3	-	-	26.7	-	-	-
	573	3.2	58.1	5.3	-	29.4	-	-	7.3
	623	11.4	39.9	6.8	-	42.9	-	-	10.4
	673	37.3	25.4	7.7	2.6	50.0	0.3	-	13.9
	723	78.1	10.0	8.4	5.7	55.3	2.1	2.1	16.3
	773	99.0	2.7	13.3	16.4	37.1	9.6	9.5	11.4
ZnO	473	0	-	-	-	-	-	-	-
	523	1.0	44.6	0.0	0.0	55.4	0.0	0.0	0.0
	573	15.1	22.2	16.5	1.3	60.0	0.0	0.0	0.0
	623	47.7	5.1	24.6	5.8	63.8	0.0	0.1	0.5
	673	85.6	0.2	29.1	3.3	39.1	19.0	8.2	1.1
	723	100.0	-	14.3	5.4	6.1	49.6	21.4	3.0

Figure captions

Figure 1. IR spectra of the adsorption of CO at low temperature on $ZnAl_2O_4$ pure powder pressed disk, in the range 2300-2000 cm^{-1}. Dashed line spectrum in the presence of CO with the cell cooled by liquid N_2 (real sample temperature 130 K) and upon outgassing upon warming up to RT. In the inset, the region of hydroxyl groups is enlarged, for the activated sample and the sample in contact with CO at 130K.

Figure 2. IR spectra of the adsorption of CO_2 on $ZnAl_2O_4$ pure powder pressed disk activated at 773 K, recorded at RT and upon outgassing up to 773 K in the range 2450-2100 cm^{-1}. Dashed line spectrum is the subtraction in the presence of CO_2 at RT. In the inset, the region of hydroxyl groups is enlarged.

Figure 3. Effect of contact time (calculated at 623 K and 773 K, respectively) on ethanol conversion and main product selectivities at 623 K (left) and 773 K (right), experiments reported in Fig. 4.

Figure 4. IR spectra of the gas phase upon ethanol reaction in the IR cell in contact with a $ZnAl_2O_4$ pure powder pressed disk, by increasing reaction temperature from 373 K and 773 K.

Figure 5. IR spectra of the $ZnAl_2O_4$ pure powder pressed disk surface in ethanol reaction in the IR cell by increasing reaction temperature from 373 K and 773 K.

Figure 6. Diffuse reflectance UV-Vis spectra of the spent catalysts after experiments at different space velocities, recorded with the pure powders versus $BaSO_4$ reference.

References

1 Limayem A, Ricke SC (2012) Prog. Energy Combust. Sci. 38:449-467

2 Balat M (2011) Energy Convers. Manag. 52:858-875

3 Mohsenzadeh A, Zamani A, Taherzadeh MJ (2017) Chem. Bio. Eng. Rev. 4:75-81

4 Phung TK, Proietti Hernández L, Lagazzo A, Busca G (2015) Appl. Catal. A Gen. 493:77-89

5 Fujita S, Iwasa N, Tani H, Nomura W, Arai M, Takezawa N (2001) React. Kinet. Catal. Lett. 73:367-372

6 Chung MJ, Han SH, Park KY, Ihm SK (1993) J. Mol. Cat. 79:335-345

7 Wang C, Garbarino G, Allard LF, Wilson F, Busca G, Flytzani-Stephanopoulos M (2016) ACS Catal. 6:210-218

8 Nakajima T, Tanabe K, Yamaguchi T, Matsuzaki T (1987) J. Chem. Soc. Chem. Comm. 294-295

9 Inui K, Kurabayashi T, Sato S (2002) Appl. Catal. A: Gen. 237:53–61

10 Larina OV, Kyriienko PI, Soloviev SO (2015) Catal. Lett.145:1162–1168

11 Bhattacharyya SK, Ganguly ND (1962) J. Appl. Chem 12:105-110

12 McKetta J (1993) Chemical Processing Handbook, Wiley, pp. 786-789

13 Phung TK, Lagazzo A, Rivero Crespo MÁ, Sanchez Escribano V, Busca G (2014) J. Catal. 311:102-113

14 Phung TK, Herrera C, Larrubia MÁ, García-Diéguez M, Finocchio E, Alemany LJ, Busca G (2014) Appl. Catal. A: Gen. 483:41-51

15 Garbarino G, Travi I, Pani M, Carnasciali MM, Busca G (2015) Catal. Comm. 70:77-81.

16 Kieffer R, Hinderman JP, El Bacha R, Kiennemann A, Deluzarche A (1982) React. Kinet. Catal. Lett. 21:17−21.

17 DeWilde JF, Czopinski CJ, Bhan A (2014) ACS Catal. 4:4425−4433.

18 Corma A, Iborra S (2006) Adv. Catal. 49:239-302.

19 Busca G (2010) Chem. Rev. 110:2217-2249.

20 Lari GM,Desai K, Mondelli C, Pérez-Ramírez J (2016) Catal. Sci. Technol. 6:2706–2714

21 Phung TK, Proietti Hernández L, Lagazzo A, Busca G (2015) Appl. Catal. A Gen. 489:180–187

22 Eckert M, Fleischmann G, Jira R, Bolt HM, Golka K, Acetaldehyde, in Ullman's Encyclopedia of Industrial Chemistry, 2012 Wiley-VCH Verlag GmbH & Co. KGaA, Weinheim

23 Weissermel K, Arpe HJ, Industrial Organic Chemistry Wiley, 3rd ed., p. 167.

24 Shan J, Janvelyan N, Li H, Liu J, Egle TM, Ye J, Biener MM, Biener J, Friend CM, Flytzani-Stephanopoulos M (2017) Appl. Catal. B: Environ. 205:541–550

25 Wang C, Garbarino G, Allard LF, Wilson F, Busca G, Flytzani-Stephanopoulos M (2016) ACS Catal. 6:210−218

26 Tanabe K, Shimazu K, Hattori H, Shimazu KI (1979) J. Catal. 57:35-40

27 Rossi PF, Busca G, Lorenzelli V, Waquif M, Saur O, Lavalley JC (1991) Langmuir 7:2677-2681

28 Bournay L, Casanave D, Delfort B, Hillion G, Chodorge JA (2005) Catal. Today 106:190-192

29 Dimian AC, Rothenberg G (2016) Catal. Sci. Technol. 6:6097-6108.

30 Breuer W, Raths HC, US patent 5326891 (1994) to Henkel.

31 Wolf G, Burkhart B, Lauth G, Trapp H, Oftring A, US patent 5741947 (1998) to BASF.

32 Welch BM, US Patent 4620053 (1986) to Phillips Petroleum Company.

33 Li X, Zhu Z, Zhao Q, Wang L (2011) J. Hazard. Mat. 186:2089-2096

34 Staszak W, Zawadzki M, Okal J (2010) J. Alloys Comp. 492:500-507.

35 Busca G, Heterogeneous Catalytic Materials, Elsevier, 2014.

36 Thommes M, Taneko K, Neimark AV, Oliver JP, Rodriguez-Reinoso F, Roquerol J, Sing KSW (2015) Pure Appl. Chem. 87:1051-1069

37 White WB, Deangelis BA (1967) Spectrochim. Acta A23:985-995.

38 Wang SF, Sun GZ, Fang LM, Lei Li, Xiang X, Zu XT (2015) Scientific Reports 5:12849

39 Kushwaha AK (2013) Comput. Mat. Sci. 69:505-509.

40 Karazanov SE, Ravindran P, (2010) J. Am. Ceram. Soc. 93:3335-3341

41 Anand GT, Kennedy LJ, Aruldoss U, Vijaya JJ (2015) J. Mol. Struct. 1084:244–253

42 Montanari T, Sisani M, Nocchetti M, Vivani R, Herrera Delgado MC, Ramis G, Busca G, Costantino U (2010) Catal. Today 152:104–109

43 Busca G (2014) Catal. Today 226:2-13

44 Busca G (2014) Advan. Catal. 57:319-404

45 Scarano D, Bertarione S, Spoto G, Zecchina A, Otero Arean C (2001) Thin Solid Films 400:50–55

46 Liu Q, Wang L, Wang C, Qu W, Tian Z, Ma H, Wang D, Wang B, Xu Z (2013) Appl. Catal. B: Environ.136-137:210– 217

47 Busca G, Lorenzelli V (1982) Mater. Chem. 7:89-126

48 Rahman MM, Davidson SD, Sun J, Wang Y (2016) Top. Catal. 59:37-45.

49 Ghiotti G, Chiorino A, Boccuzzi F (1993) Surf. Sci. 287/288:228-234

50 Wilson HF, Barnard AS (2015) J. Phys. Chem. C 119:26560−26565

51 Phung TK, Busca G (2015) Cat. Comm., 68:110-116.

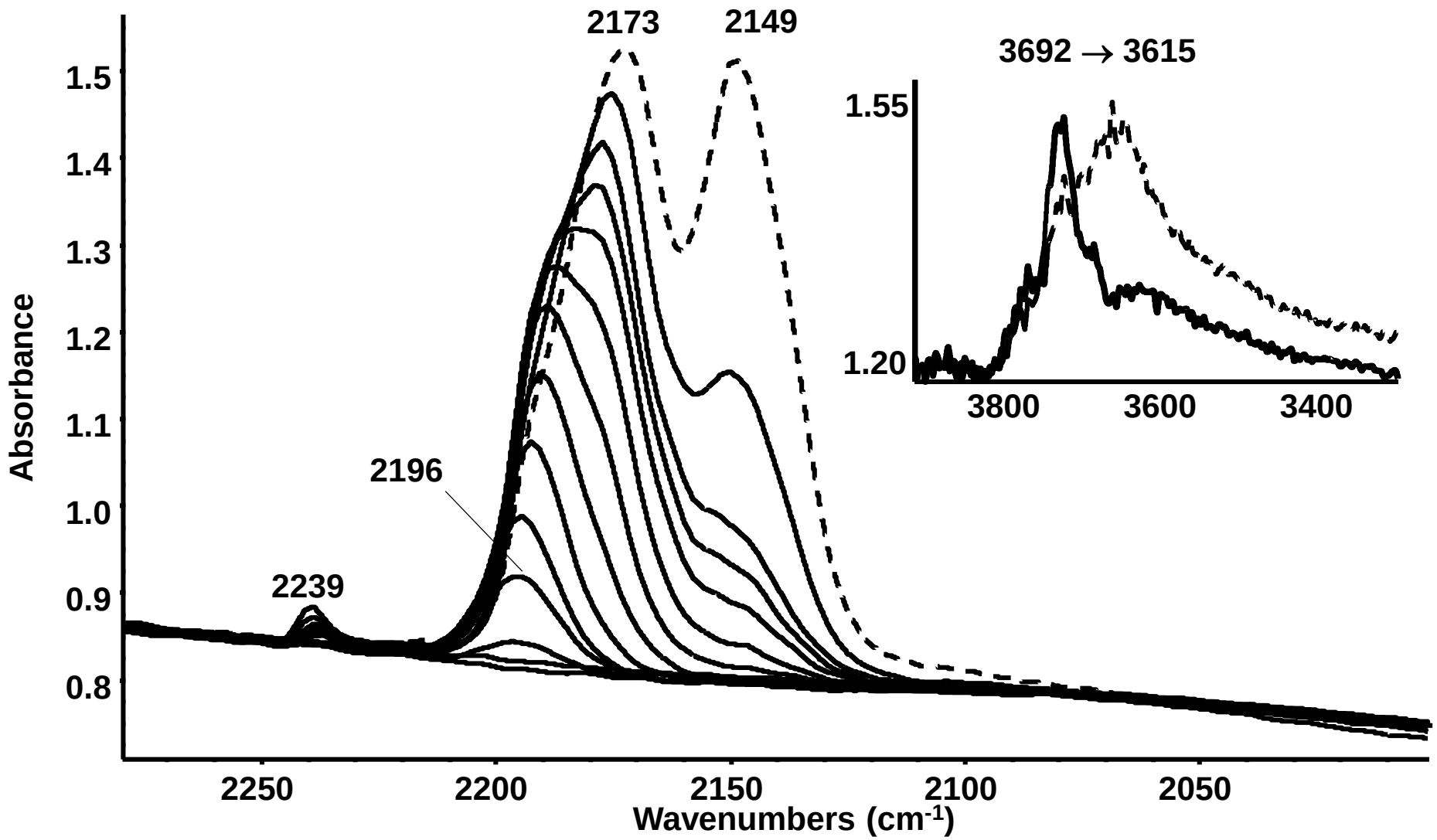
2173
2149
3692 → 3615
1.55
1.20
3800
3600
3400
2196
2239
Absorbance
1.5
1.4
1.3
1.2
1.1
1.0
0.9
0.8
2250
2200
2150
2100
2050
Wavenumbers (cm-1)

Figure 1

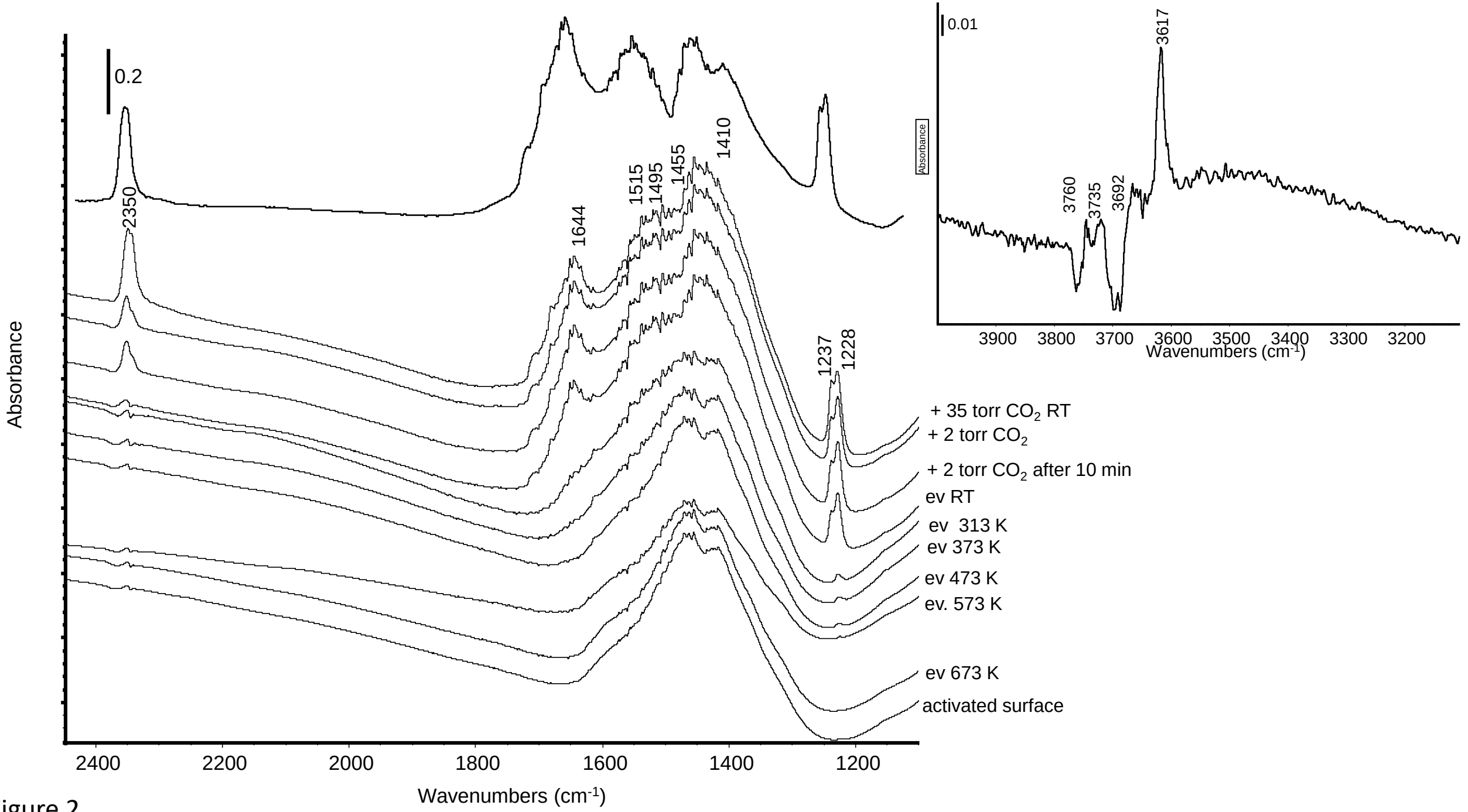
0.2
2350
1644
1515
1495
1455
1410
1237
1228
Absorbance
+ 35 torr CO_2 RT
+ 2 torr CO_2
+ 2 torr CO_2 after 10 min
ev RT
ev 313 K
ev 373 K
ev 473 K
ev. 573 K
ev 673 K
activated surface
2400
2200
2000
1800
1600
1400
1200
Wavenumbers (cm^{-1})
0.01
Absorbance
3617
3760
3735
3692
3900
3800
3700
3600
3500
3400
3300
3200
Wavenumbers (cm^{-1})

Figure 2

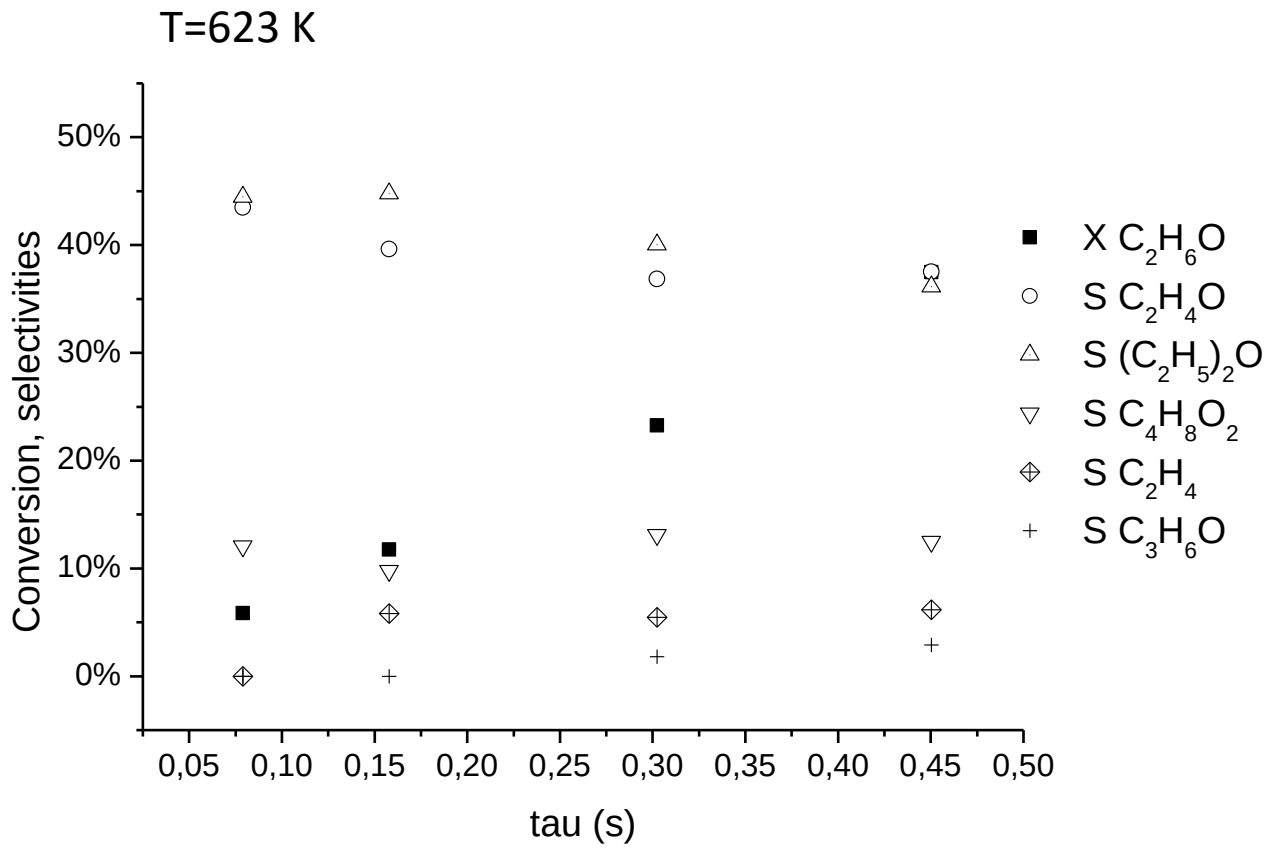
T=623 K
Conversion, selectivities
50%
40%
30%
20%
10%
0%
0,05
0,10
0,15
0,20
0,25
0,30
0,35
0,40
0,45
0,50
tau (s)
X C2H6O
S C2H4O
S (C2H5)2O
S C4H8O2
S C2H4
S C3H6O

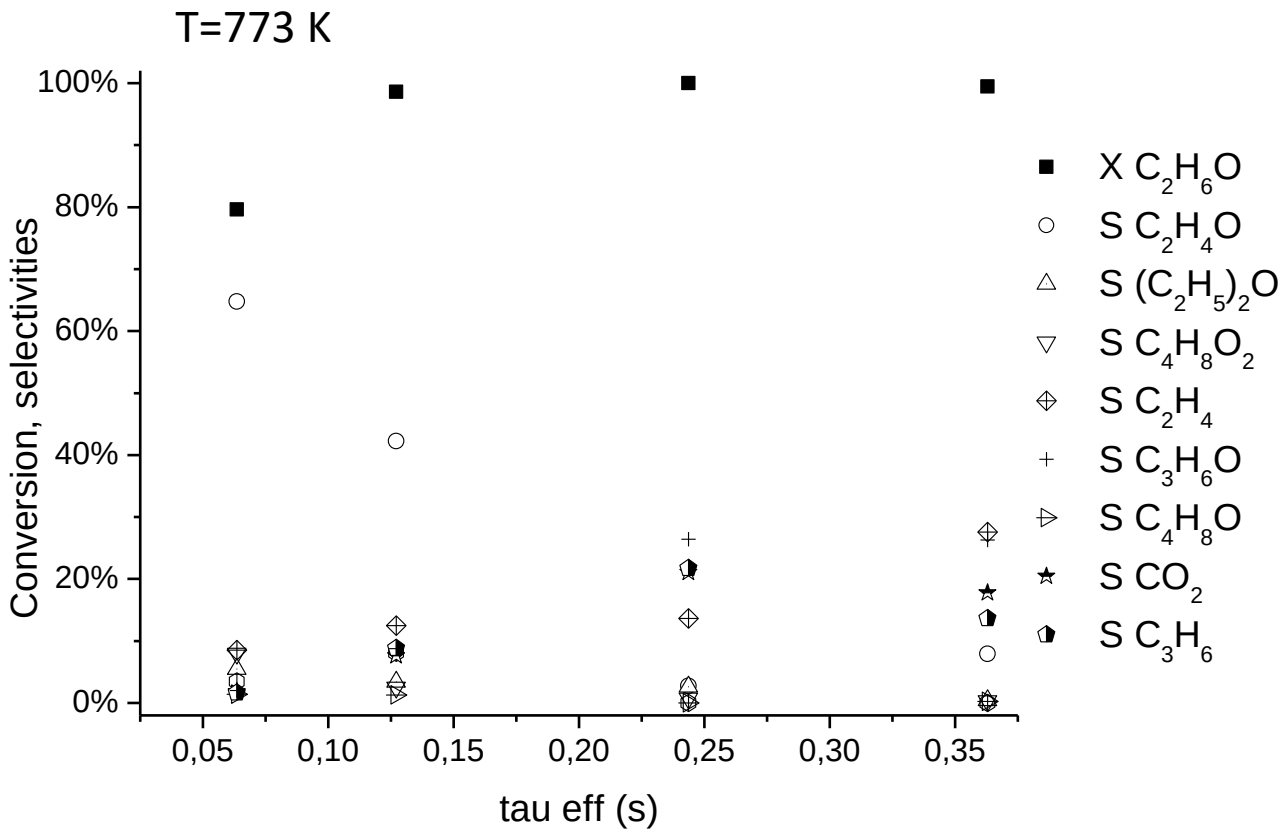
T=773 K
Conversion, selectivities
100%
80%
60%
40%
20%
0%
0,05
0,10
0,15
0,20
0,25
0,30
0,35
tau eff (s)
X C2H6O
S C2H4O
S (C2H5)2O
S C4H8O2
S C2H4
S C3H6O
S C4H8O
S CO2
S C3H6

Figure 3

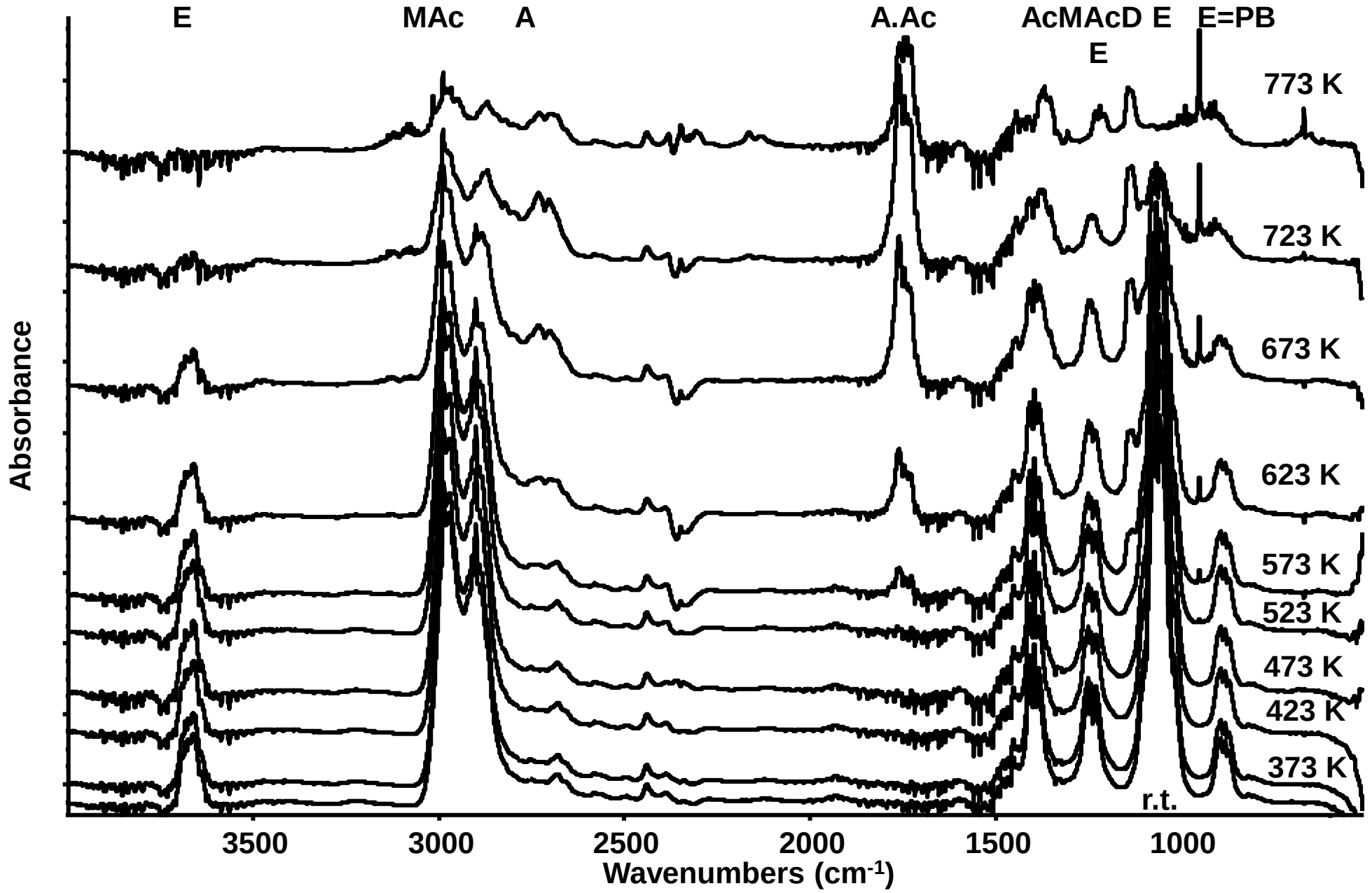
E
MAc
A
A.Ac
AcMAcD E
E
E=PB
773 K
723 K
673 K
623 K
573 K
523 K
473 K
423 K
373 K
r.t.
Absorbance
3500
3000
2500
2000
1500
1000
Wavenumbers (cm-1)

Figure 4

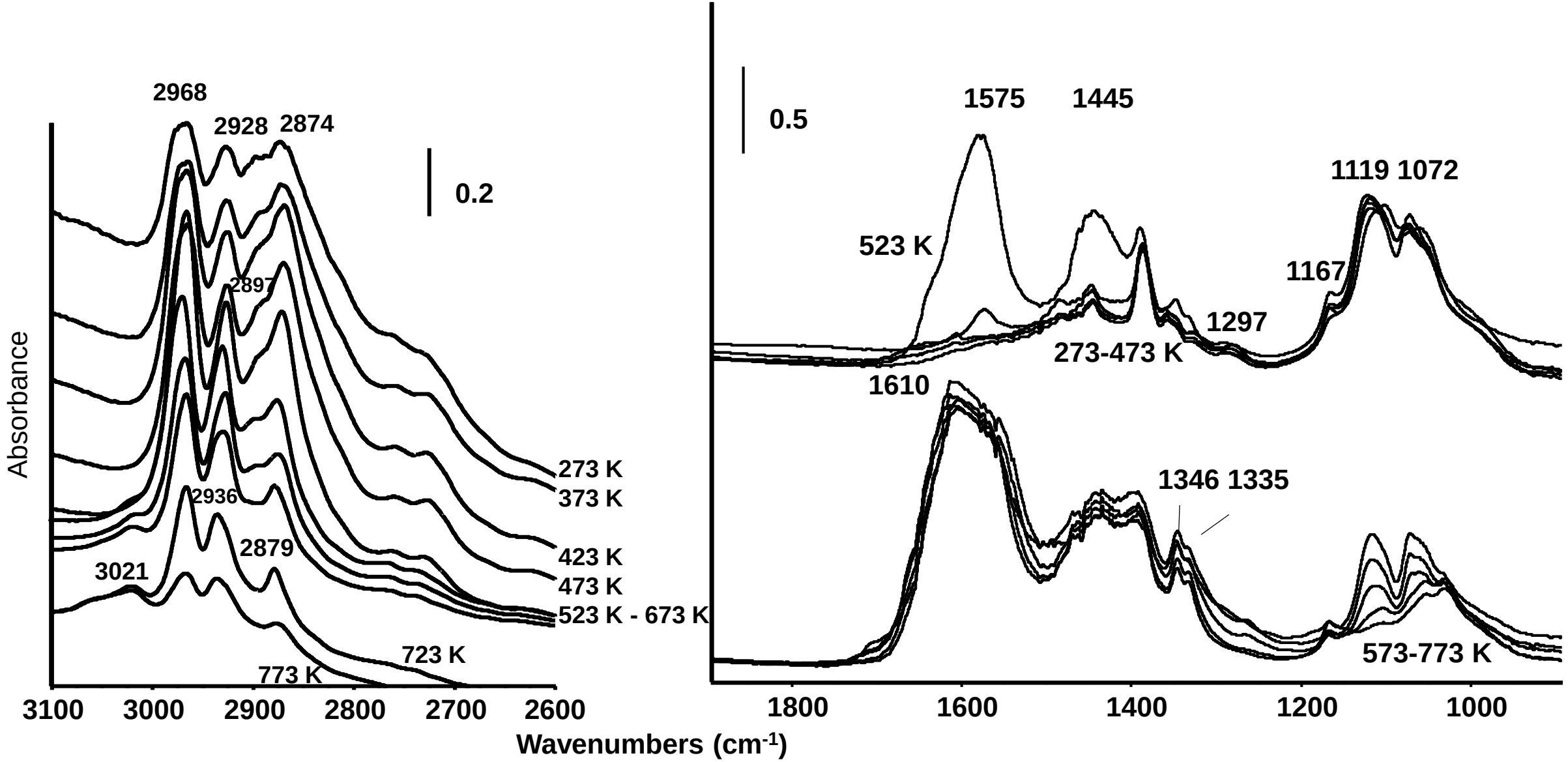
2968
2928
2874
0.2
2897
2936
2879
3021
273 K
373 K
423 K
473 K
523 K - 673 K
723 K
773 K
Absorbance
3100
3000
2900
2800
2700
2600
0.5
1575
1445
1119 1072
523 K
1167
1297
273-473 K
1610
1346 1335
573-773 K
1800
1600
1400
1200
1000
Wavenumbers (cm-1)

Figure 5

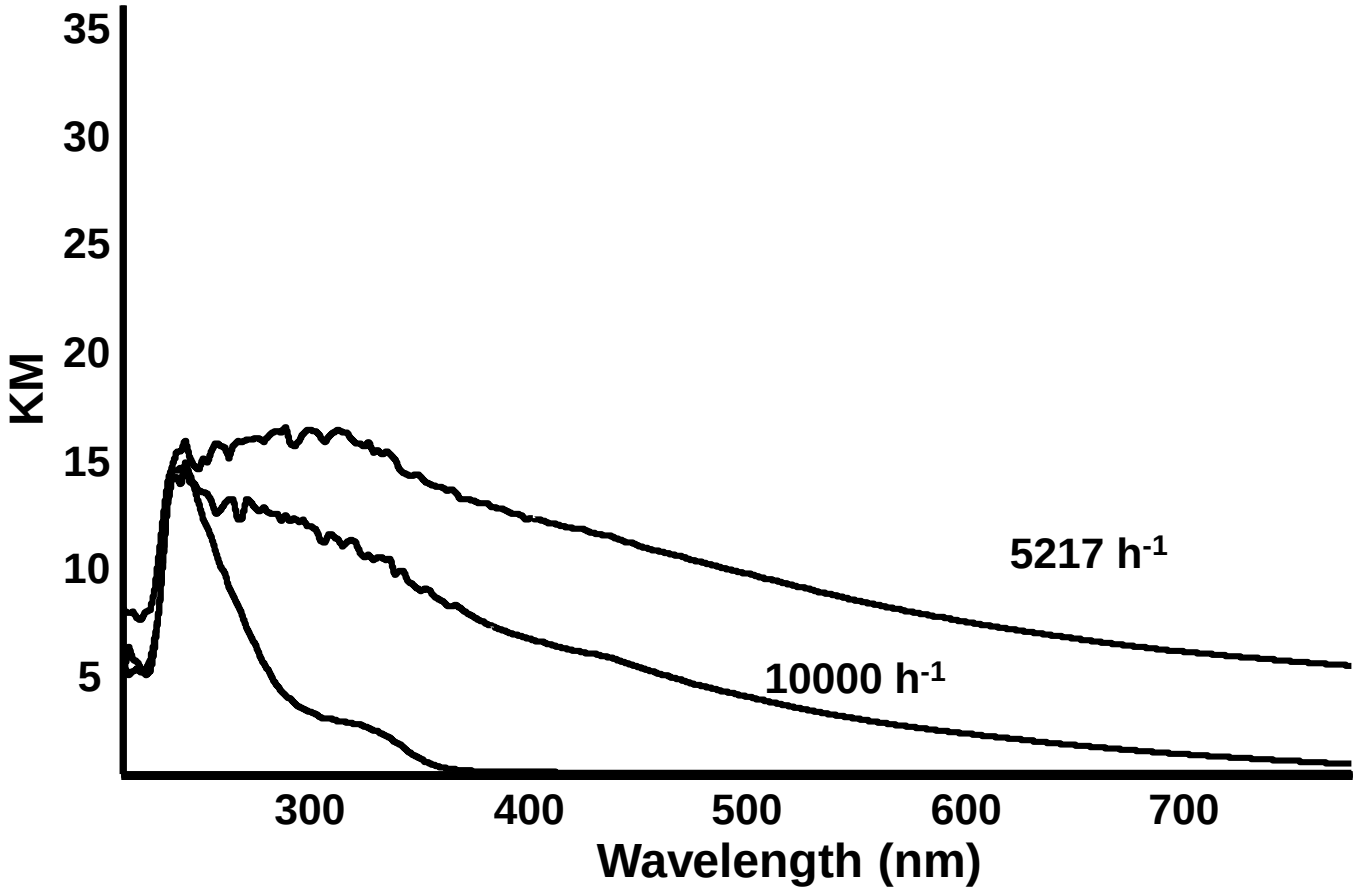
35
30
25
20
15
10
5
KM
5217 h-1
10000 h-1
300
400
500
600
700
Wavelength (nm)

Figure 6